

Exhumation, Rift-flank Uplift, and the Thermal Evolution of the Rwenzori Mountains  
Determined by Combined (U-Th)/He and U-Pb Thermochronometry

by

Daniel MacPhee

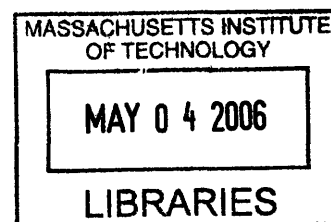
B.S. Geology and Geophysics  
Yale University, 2001

SUBMITTED TO THE DEPARTMENT OF EARTH, ATMOSPHERIC, AND PLANETARY  
SCIENCE IN PARTIAL FULFILLMENT OF THE REQUIREMENTS FOR THE DEGREE OF

MASTER OF SCIENCE IN EARTH AND PLANETARY SCIENCES  
AT THE  
MASSACHUSETTS INSTITUTE OF TECHNOLOGY

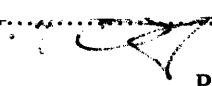
FEBRUARY 2006

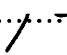
© 2006 Massachusetts Institute of Technology  
All rights reserved.



**ARCHIVES**

Signature of Author.....  
Department of Earth, Atmospheric, and Planetary Science  
February 6, 2006

Certified by.....  
  
Samuel A. Bowring  
Professor of Geology  
Thesis Supervisor

Accepted by.....  
  
Maria T. Zuber  
E.A. Griswold Professor of Geophysics  
Head, Department of Earth, Atmospheric, and Planetary Sciences



Exhumation, Rift-flank Uplift, and the Thermal Evolution of the Rwenzori Mountains  
Determined by Combined (U-Th)/He and U-Pb Thermochronometry

by

Daniel MacPhee

Submitted to the Department of Earth, Atmospheric, and Planetary Science on February 6, 2006  
in Partial Fulfillment of the Requirements for the Degree of Master of Science in Earth and  
Planetary Sciences

**ABSTRACT**

Rising over 5 km along the border of Uganda and the Democratic Republic of the Congo, the Rwenzori Mountains represent an extreme example of basement rift-flank uplift in the western branch of the East African Rift, a phenomenon common throughout the East African Rift System and characteristic of continental rift systems in general. A thermochronologic study combining (U-Th)/He and U-Pb analysis of apatite, titanite, and zircon separated from crystalline basement rocks was conducted across the Rwenzori block to characterize the timing and rate of rift-flank exhumation related to continental extension in east-central Africa. The thermochronologic data coupled with field and remote sensing observations make the case for recent and non-steady state uplift of the massif. Uranium-lead thermochronology indicate that, prior to Upper Neogene rifting, the rocks of the Rwenzori experienced a protracted history of slow cooling without major tectonothermal perturbation since at least the Paleoproterozoic (ca. 1900 Ma). Stream channel steepness profiles and thermochronometry along the western slope of the range show it to be the main active scarp that accommodates uplift. Relatively old (U-Th)/He zircon and apatite dates (>400 Ma, >70 Ma respectively) along the high peaks and eastern slope of the range reflect a transient lag period resulting from yet-insufficient exhumation to remove the inherited pre-rift cratonic thermal structure. This non-steady state condition of rapid uplift outpacing erosion has resulted in preservation of relict landsurfaces, truncated spurs, hanging valleys, uplifted river terraces, and vast stranded bogs at high elevation. Given the low cooling rate and geothermal gradient prior to rifting implied by U-Pb thermochronometry we determine that no more than 1.7 km of erosion could have accompanied uplift on the order of at least 5 km in the Rwenzori region. Biostratigraphic evidence suggests the range rose from beneath local baselevel within the last 2.5 Ma. This requires a minimum average uplift rate of 1.6 km/Myr. Regardless of the active rock uplift rate of the Rwenzori, net exhumation cannot yet have exceeded the depth of the (U-Th)/He closure isotherm in apatite (<1.7 km). These results highlight the danger of modeling young orogenic systems using the simplifying assumption of topographic steady state.

Thesis Supervisor: Samuel A. Bowring  
Title: Professor of Geology



## **TITLE**

Exhumation, rift-flank uplift, and the thermal evolution of the Rwenzori Mountains determined by combined (U-Th)/He and U-Pb thermochronometry

## **ABSTRACT**

Rising over 5 km along the border of Uganda and the Democratic Republic of the Congo, the Rwenzori Mountains represent an extreme example of basement rift-flank uplift in the western branch of the East African Rift, a phenomenon common throughout the East African Rift System and characteristic of continental rift systems in general. A thermochronologic study combining (U-Th)/He and U-Pb analysis of apatite, titanite, and zircon separated from crystalline basement rocks was conducted across the Rwenzori block to characterize the timing and rate of rift-flank exhumation related to continental extension in east-central Africa. The thermochronologic data coupled with field and remote sensing observations make the case for recent and non-steady state uplift of the massif. Uranium-lead thermochronology indicate that, prior to Upper Neogene rifting, the rocks of the Rwenzori experienced a protracted history of slow cooling without major tectonothermal perturbation since at least the Paleoproterozoic (ca. 1900 Ma). Stream channel steepness profiles and thermochronometry along the western slope of the range show it to be the main active scarp that accommodates uplift. Relatively old (U-Th)/He zircon and apatite dates (>400 Ma, >70 Ma respectively) along the high peaks and eastern slope of the range reflect a transient lag period resulting from yet-insufficient exhumation to remove the inherited pre-rift cratonic thermal structure. This non-steady state condition of rapid uplift outpacing erosion has resulted in preservation of relict landsurfaces, truncated spurs, hanging valleys, uplifted river terraces, and vast stranded bogs at high elevation. Given the low cooling rate and geothermal gradient prior to rifting implied by U-Pb thermochronometry we determine that no more than 1.7 km of erosion could have accompanied uplift on the order of at least 5 km in the Rwenzori region. Biostratigraphic evidence suggests the range rose from beneath local baselevel within the last 2.5 Ma. This requires a minimum average uplift rate of 1.6 km/Myr. Regardless of the active rock uplift rate of the Rwenzori, net exhumation cannot yet have exceeded the depth of the (U-Th)/He closure isotherm in apatite (<1.7 km). These

results highlight the danger of modeling young orogenic systems using the simplifying assumption of topographic steady state.

## **INTRODUCTION**

Low temperature (U-Th)/He thermochronometry is used to examine the late Cenozoic history of uplift and exhumation of the Precambrian Rwenzori massif in east-central Africa. Reaching elevations over 5000 m, the Rwenzori have the distinction of the third highest elevation in Africa, surpassed only by the singular volcanic peaks of Mt. Kilimanjaro and Mt. Kenya. But unlike their constructional topography situated at the center of the East African Rift Valley, the Rwenzori comprise a 130 km by 50 km block of uplifted Archean-Paleoproterozoic West Nile basement--granitoids, schists, and gneisses--forming a rift-flank more than 4000 m above the adjacent Albertine basin at the northernmost extent of the Western Branch of the East African Rift System (EARS). Flank uplifts are characteristic features of continental rifts that have been extensively studied by previous workers in ancient and mature active settings (e.g. House et al., 2003; Watts et al., 1982; van der Beek et al., 1994). The Rwenzori present a unique opportunity to study the evolution of rift-flank uplift in its nascent stages and with an unusually large magnitude of uplift. In this study we use thermochronometry to better constrain the larger geodynamic questions implicit in the sudden uplift of a massive block of stable cratonic lithosphere in a setting of regional continental extension. When did they form? How fast did they rise, and by what mechanism? What asthenosphere-lithosphere interactions are involved; did pre-existing boundaries in the lithospheric mantle below the Rwenzori have any influence on the size, magnitude or velocity of uplift?

## **THE EAST AFRICAN RIFT SYSTEM**

The East African Rift System stretches more than 3500 km from the Afar triple junction **south**, through the mouth of the Zambezi River in Mozambique (Figure 1). The rift system **largely** follows a zone defined by anastomosing Proterozoic orogenic belts that weld together Archean cratonic fragments, most notably bifurcating into an eastern and western branch at the northern end of Lake Malawi to pass around the Tanzania Craton. The Eastern Branch, or Gregory Rift, is the older (ca.20 Ma), wider (50-80 km), and better studied of these two arms, although much of its early stratigraphic record lies buried beneath voluminous volcanic rocks

(Baker et al., 1971). In contrast, the younger (<12 Ma), narrower (40-50 km), Western Branch of the EARS is characterized by limited extrusive volcanism though its deep, long-lived, lacustrine basins record a nearly complete sedimentary record back through the Miocene (Laerdal and Talbot, 2002; Pickford et al., 1992).

Today much of eastern Africa comprises a broad topographic swell averaging >1000 m elevation. However, prior to rift initiation, as far back as the early Cenozoic, much of eastern Africa was a lowland area (<500 m) dominated by extensive peneplains (Michot, 1934; Dixey, 1945; Hepworth, 1962; Ollier, 1990; Stankiewicz and de Wit, 2006). Continentally-derived Early Miocene sediments deposited in the Indian Ocean along the Tanzanian passive margin are the first indication of uplift and erosion of the East African Plateau in response to the impinging Afar plume (Saggerson and Baker, 1965). Deposition was contemporaneous with initial volcanism in the Gregory Rift at 23 Ma (Baker et al., 1971) and preceded active rift faulting at ca. 17 Ma (Shackleton, 1951; Drake et al., 1988). In the few cases where relative timing has been reliably established, normal faulting and flank-uplift is found to lag behind initial volcanism and regional uplift (Gregory Rift segments: Lotikipi Plain- Morley et al., 1992; Turkana- Baker et al., 1988; Bellini, 1981). Volcanism in the Western Branch of the EARS began around 12 Ma in Ruizi segment of Rwanda-Burundi, but the earliest preserved extrusive volcanism in the Albertine segment is not until the latest Pleistocene (Kampunzu et al., 1998; Ebinger et al., 1989a,b).

A series of en echelon asymmetric graben subdivide the EARS into segments typically 80-130 km in length, connected by oblique-slip transfer faults. Polarity of maximum displacement generally alternates from eastern to western boundary faults along strike. Often, a steep scarp rising hundreds to thousands of meters above the graben floor defines the dominant boundary fault in each basin while the facing subordinate valley wall is usually a lesser scarp or upwarp without clear surface rupture. The Rwenzori massif is the most extreme example of rift-flank uplift in the EARS, towering more than 4 km above the eastern edge of the Semliki River plain in the Albertine Basin. Including a buried sedimentary section exceeding 4 km in the central axis of the rift basin, more than 8 km of structural relief is involved (Kiconco, 2005).

## **THE ALBERTINE BASIN AND RWENZORI MOUNTAINS**

Extension began as early as 8 Ma in the Western Branch of the East African Rift (e.g. Ebinger, 1989b; McConnell, 1972; and references therein). There is abundant evidence, however, to suggest that the uplift of the Rwenzori block occurred even more recently. The Albertine Rift basin is often considered the oldest segment of the Western Branch of the EARS based on an assumption that southerly rift propagation occurred from its position at the northernmost terminus of the Western Branch. While it is likely that early stages of extension were underway in the Albertine basin by the end of the Miocene, it is certainly not likely that any rift-flanks of significant topographic relief existed until well later in the rift's evolution. The Albertine basin exhibits a half-graben morphology typical of the Western Branch rift basins with marked rift-flank uplift along its eastern boundary fault to form the Rwenzori massif. All known volcanism in the Albertine Basin is younger than 0.05 Ma (Boven et al., 1998). The range is the most seismically active region in East Africa, with seismic events occurring not only along the major boundary faults, but also beneath the Rwenzori block itself (Maasha, 1975a,b). Major drainage reorganization occurred in the middle Pleistocene when flank uplift in the Albertine Rift cut off westward drainage into the Congo Basin, creating Lakes Victoria and Kyoga as flow stagnated. Eventually the whole region was captured to become part of the north-draining Nile Basin (Beadle, 1981; Doornkamp et al., 1966). Vicariance of fossil mollusks in the Albertine Basin suggests that Lakes Albert and Edward/George existed as a single large lake until about 2.5 Ma, consistent with the assertion that the region was relatively flat-lying prior to the development of relief in the Rwenzori range (Van Damme and Pickford, 2003). Paleobotanical reconstructions indicate that the East African Plateau was below 500 m elevation in this region up until the Miocene at least (Hopwood and Lepersomme, 1953). Presently this regional plateau surface is at ca. 1000 m elevation above which the Rwenzori rise up to 5109 m. Truncated spurs, hanging valleys, uplifted river terraces, and vast stranded bogs at high elevation attest to the geomorphic youth of the range (Figure 2; e.g. Egoroff, 1966; Whittow, 1966; Filippi, 1908). Though deeply dissected by a few major rivers with boulder-choked beds, much of the eastern slopes of the Rwenzori can be characterized by a series of gently-dipping relict surfaces often correlated by earlier workers to the Jurassic to mid-Tertiary peneplain surfaces of Wayland (1934) and McConnell (1959) that are prominent throughout the rest of Uganda.



## **THERMOCHRONOMETRY: THEORY, METHODS, SAMPLING**

Thermochronometry exploits the temperature-dependent diffusion rates of radiogenic daughter nuclides through a mineral lattice as a means of recording the duration of time an analyzed mineral grain last cooled below its bulk closure temperature ( $T_{cb}$ ). The concept of bulk closure temperature was derived by Dodson (1973) and has been used extensively as an effective tool for tracking the thermal evolution of orogens, the timing of metamorphic events, or for studies of exhumation and near-surface processes. The number of useful thermochronologic mineral-isotope systems has increased in recent years, offering the potential to obtain cooling dates from a wide range of rock types and closure temperatures (see Hodges, 2003 for review of systems and nominal  $T_{cb}$ s). Despite the apparent elegance of the theory, there are many important assumptions that must be met, and analytical complexities that must be overcome before interpreting thermochronometric data. For example, Dodson's approach assumes steady monotonic cooling, transport of radiogenic daughter products through the mineral exclusively by volume diffusion, an infinite negative chemical gradient for the daughter at the grain boundary, and no loss of radiogenic parent isotopes except by radioactive decay. Each mineral-isotope system has a nominal closure temperature that is critically dependent on factors such as grain size and shape, and cooling rate:

$$T_{cb} = E / ( R \ln ( e^{G_{av}} R D_i T_{cb}^2 / a^2 E (dT/dt) ) )$$

where  $T_{cb}$  = whole-grain bulk closure temperature  
E = activation energy  
R = universal gas constant  
 $G_{av}$  = grain-geometry function  
 $D_i$  = diffusivity at infinite temperature  
a = effective diffusion dimension  
dT/dt = cooling rate

Parameters such as grain size and cooling rate can vary widely depending on tectonic setting and must be addressed in order to assure proper interpretation of calculated dates. In the case of stable cratonic lithosphere, these effects are greatly magnified because often inherently low geothermal gradients are compounded by extremely slow exhumation rates which act together to amplify small differences in physical diffusion parameters between individual grains or slight spatial heterogeneities in tectonic histories that add up over a protracted period of ingrowth to produce large disparities in measured ages. The most important example of the sorts

of complications that can arise is the concept of a partial retention zone (PRZ). Analogous to the partial annealing zone used in fission track dating, the PRZ is a temperature interval defined for each mineral-isotope system over which a mineral grain goes from virtually instantaneous loss of all produced daughter isotopes to complete retention of all daughter products (House et al., 1999; Wolf et al., 1998). Depending on the rock uplift rate, regional cooling rate, and geothermal gradient, the PRZ can span a wide range of depth and/or temperatures. Likewise, a rock may pass through the PRZ very quickly in the case of rapid exhumation and cooling (e.g. Batt, 2001), or remain in it for hundreds of millions of years as in the case of cratonic interiors (e.g. Flowers et al., submitted)

Because we are principally interested in the recent exhumation of an ancient landsurface, it is especially important to quantify the pre-uplift thermal structure of the lithosphere in order to determine a reasonable bulk closure temperature estimate for apatite and zircon (U-Th)/He thermochronometry (AHe and ZHe respectively). Using high- to medium-temperature U-Pb thermochronology we determine the long-term regional cooling rate ( $dT/dt$ ) which is used, along with individual grain size measurements, to calculate an accurate effective  $T_{cb}$ . Since the West Nile lithosphere has had a long history of stability and slow cooling since the Paleoproterozoic, the expected  $T_{cb}$ s for AHe and ZHe are ca. 50 °C and ca. 150 °C respectively (significantly lower than the nominal  $T_{cb}$ s of ca. 70 °C and ca. 180-200 °C typically assumed for active convergent orogenic settings with higher cooling rates). Figure 3 illustrates the decrease in effective bulk closure temperature of the (U-Th)/He system caused by lowering cooling rate for a typical range of grain sizes or the geothermal gradient.

We use the multichronometer approach described above to track the thermal evolution of crystalline basement samples from high temperature igneous crystallization to low temperature near-surface exposure using a combination of U-Pb and (U-Th)/He dating of zircon, titanite, and apatite. To do this, a suite of rocks were collected during fieldwork in Uganda in 2003 and augmented by a set of samples from the Congolese slope of the Rwenzori originally collected by the joint British-Ugandan Geological Expedition of 1951-1952 led by WQ Kennedy. This study focuses on a subset of seven of these samples selected for optimal geographic coverage as well as containing the requisite mineralogy. The samples are from both sides of the range and from elevations below the base on the East African Plateau surface at 690 m up to the edge of glacial

cover in the central high peaks at 4600 m. Accessory minerals were separated by standard crushing, magnetic, and density techniques prior to hand-picking of inclusion-free, euhedral (when possible) grains for dating. Single grain (and, in some cases, subgrain) analyses were done by ID-TIMS at MIT for U-Pb dating and by LA-ICPMS for U-Th-He at Yale University. The approximate bulk closure temperatures for each mineral-isotope system are plotted along with a generalized regional cooling curve derived from the compiled geochronologic data in Table 1. Cooling dates over a wide range of closure temperatures allows us to characterize the pre-rift geotherm with medium- to high temperature U-Pb thermochronometry while simultaneously tracking recent perturbation of this inherited thermal structure during uplift with the low temperature (U-Th)/He thermochronometers.

## **RESULTS**

U-Pb and (U-Th)/He thermochronometry results from samples collected from the Rwenzori Block of the West Nile Terrane of Uganda and the Democratic Republic of the Congo are tabulated in Tables 1 and 2. Immediately apparent in all samples is the great antiquity recorded by all thermochronometers. In the U-Pb system, zircon preserves Late Archean crystallization ages followed by relatively rapid cooling through the closure temperature of titanite, and in some places apatite, prior to a thermal resetting of most apatite and a new generation of titanite growth coincident with the Paleoproterozoic deformation of the Rwenzori Fold Belt, followed by an extended period of slow cooling. Most surprisingly, the (U-Th)/He ages show a similar continuation of this ancient slow cooling--ca. 400 Ma in zircon and >70 Ma in apatite. The broad implication is that after crystallization of the West Nile Region between 2620-2510 Ma, the rocks have been below the closure temperature for Pb-diffusion in apatite (ca. 450 °C) for at least 1900 My, and below the temperature for He-diffusion in apatite (ca. 50 °C) for more than 70 My. This suggests that the rocks of the Rwenzori block, like the rest of the West Nile Terrane, have had a protracted history of slow cooling without major perturbation since at least the Paleoproterozoic. Furthermore, AHe ages in excess of 70 Ma found at the landsurface today constrain the total exhumation across the region since the Cretaceous to a maximum limit of <2 km. This apparently slow exhumation may not be surprising for a fragment of cratonic lithosphere in the context of the African continent, which has been

stationary and nearly surrounded by passive margins at least through the Cenozoic, but it is not at all expected in the context of a glaciated mountain range with more than 4000 m of local relief in one of the wettest climates of the world.

## **U-Pb RESULTS**

Typical of cratonic lithosphere, the history of the Archean West Nile terrane is one of relatively rapid post-orogenic cooling followed by a long quiescent period of tectonothermal stability characterized by a low-gradient geotherm (ca. 20 °C/km) and extremely slow exhumation (<15 m/My). Figure 4 is a generalized regional cooling curve that integrates our results for U-Pb analyses of zircon, titanite, and apatite grains (Table 1). Uranium-lead zircon geochronology records Late Archean crystallization of the constituent terranes of the West Nile lithosphere between 2620-2510 Ma, followed by moderate cooling (ca. 5-15 °C/My) (Table 1) through the closure temperature of titanite and apatite (ca. 650 °C and 450 °C respectively). Nearly pervasive thermal resetting (or new growth) of apatite and a new generation of titanite growth mark the effect of a ca. 1900 Ma upper-greenschist facies regional metamorphic event that brought a renewed episode of rapid cooling. The thermal perturbation associated with deformation was brief enough to produce identical U-Pb apatite dates despite large grain-size variations suggesting cooling well below ca. 450 °C. The maximum effective regional temperature of this orogenic event is constrained to be between 450 °C and 650 °C because extant titanite grains were unaffected by the thermal pulse. These data give a robust age to the 'Rwenzori Fold Belt' described by Tanner (1971) and Cahen and Snelling (1984) that stretches across southern Uganda and well into the Congo separating the Tanzania and West Nile cratons. This was the last major tectonothermal disturbance of the West Nile terrane before it achieved a stable thermal structure which persisted until initiation of rifting in the late Miocene. Thus, since the Paleoproterozoic the West Nile Terrane has remained stable--slowly cooling (<0.5 °C/My), with no evidence of major regional reactivation during the Kibaran orogeny (ca. 1300 Ma) to the south in nearby Rwanda/Burundi, and the Pan African (ca. 800-650 Ma) thermotectonism of the East African Orogen to the east, in Kenya and Tanzania. This bears testimony to the remarkable stability and longevity of cratonic lithosphere as documented similarly for other regions (e.g. Schmitz and Bowring, 2003). Clearly, with the Rwenzori now uplifted more than 5 km above

sea level and Lakes Albert and Edward filled with Miocene and younger sediments totaling more than 4km, this long-lived stability has been catastrophically perturbed. Using the thermal structure determined from U-Pb thermochronology as an initial condition, we turn to the low-temperature sensitivity of (U-Th)/He thermochronometry to elucidate the timing and rate of recent exhumation of this ancient stable craton to form the Rwenzori Massif.

## **(U-Th)/He RESULTS**

U-Th-He data from seven samples with both apatite and zircon grains, indicate closure dates that vastly exceed that of rifting in the Albertine Basin (Table 2). Apatite (U-Th)/He dates range from 19-186Ma and zircon (U-Th)/He dates are uniformly older, falling between 238-462 Ma. Even without consideration of the punctuated pulse of exhumation caused by recent uplift of the Rwenzori, these ages imply maximal long-term cooling rates of  $<0.5$  °C/My and decreasing with time. With the exception of the Miocene ages recorded by sample R416, all AHe dates are Cretaceous in age. Similarly, ZHe ages fall into one main middle Paleozoic population of 350-430 Ma with the exception of R416 that gives significantly younger end-Paleozoic ages ca. 250 Ma.

A first-order conclusion that can be drawn from these data is that they record a continuation into at least the uppermost Mesozoic of the same slow cooling determined by U-Pb thermochronometry. Taken at face value, the ages imply maximal long-term cooling rates of  $<0.5$  °C/My, consistent with maturation of Archean lithosphere. However, the Rwenzori Mountains, as we see them today, are anything but a typical expanse of flat continental shield. Unfortunately, despite their extremely steep relief, they are in such a nascent stage of topographic development that they do not yet expose 'young' (U-Th)/He ages set at the time of uplift initiation. This is well illustrated by a complete lack of correlation between cooling age and sample elevation within the range (Figure 5). Most low-temperature thermochronometric studies equate initiation of uplift with a break in slope in a linear age-elevation plot (e.g. Braun, 2002; Reiners and Brandon, 2006). In doing so, they abide by the assumption that orogenesis is a steady-state process--spatially, temporally, and, most importantly, thermodynamically through all levels of the lithosphere. In many ancient and mature convergent orogens these assumptions are acceptable approximations, and age-elevation plots serve us well, but in situations of constructive topography and significant advective heat transfer, these assumptions do not hold.

## **DISCUSSION & IMPLICATIONS**

### **Implication of 'old' He-dates for Rwenzori Uplift/Exhumation - 3 Models**

Figure 6 shows three basic conceptual models depicting possible combinations of uplift and erosion responsible for the formation of the present landscape of the Rwenzori massif. Based on U-Pb mineral-pair thermochronometry (and further substantiated by (U-Th)/He thermochronometry) we take 0.5 °C/My as a reasonable upper estimate of the long term cooling rate experienced by rocks of the West Nile Terrane in order to calculate appropriate AHe and ZHe bulk closure temperatures taking the radius of a single grain as the effective diffusion dimension. With a typical cratonic geothermal gradient of 20 °C/km and average surface temperature of 15 °C, an approximate depth to their respective closure isotherms is then determined at ca. 1.7 km for AHe and ca. 6.7 km for ZHe.

In order to account for the (U-Th)/He data, we must select a scenario that limits the magnitude of net exhumation since uplift to less than the depth to the AHe closure isotherm prior to uplift (<2 km). Model A depicts a scenario whereby large magnitude exhumation is achieved by a combination of high rock uplift rates and high erosion rates--a regime often invoked for mountain ranges with high relief and erosive potential like the Rwenzori (e.g. Batt et al., 2001; Willet, et al., 2001). Because we do not find evidence for deep exhumation at the present-day surface anywhere in the Rwenzori (e.g. no young ages reflecting Upper Neogene uplift), such a model can be ruled out. In order to satisfy the constraint of <2 km total exhumation while still accounting for uplift on the order of 5 km, we are left with two diametrically opposed scenarios that could fit the thermochronologic results. First, Model B is a topographic steady state scenario which describes the Rwenzori as an ancient mountain range being slowly exhumed. Alternatively, Model C is a non-steady state condition where erosion across the Rwenzori block has been outpaced by rapid, recent uplift. Both the latter models result in broadly similar thermal structure exposed at the present-day landsurface despite their completely different tectonic histories and thermal structures at depth. The critical difference between these two possible models lies in the structure of the geotherm. In Model B, the rate of rock uplift is sufficiently slow to allow for continual equilibration of a conductive geotherm in which the depth beneath the geoid to the 50°C AHe closure isotherm remains fixed through time despite long-term rock

uplift, erosion, and exhumation at the landsurface. In contrast, the non-steady state Model C depicts upward advection of isotherms because the timescale for conductive thermal relaxation of the geotherm is exceeded by the rate of uplift of the landsurface. This has the effect of physically translating the ancient geotherm upwards within the ascending rift-flank without exposing 'young' (U-Th)/He ages at the landsurface until sufficient erosion has occurred to exhume their paleo-closure isotherm.

Given the physical evidence of the youth of the range outlined above, and the exceptionally slow rate of erosion required to retain >70 Ma He-apatite ages at the landsurface (<25 m/Myr), it seems more likely that the apparently 'old' surface ages of the Rwenzori merely represent a transient lag period before sufficient exhumation has occurred to erode away the inherited pre-rift thermal structure. For a typical cratonic geothermal gradient of 20 °C/km, a long-term cooling rate of 0.5 °C/My, and average surface temperature of 15 °C, ca. 1.7 km of denudation must occur in order to exhume apatite from below its 50 °C closure isotherm with a cooling rate of 0.5 °C/My, while ca. 6.7 km is required for zircon to ascend from its 150°C closure isotherm. This requires that <2 km of erosion has accompanied uplift on the order of 5-8 km in the Rwenzori region--a plausible scenario if the absolute rate of rock uplift vastly exceeds erosion to allow for the initial development of relief. These results highlight the danger of modeling young orogenic systems using the simplifying assumptions of topographic steady state.

### **Effect of protracted, slow cooling on (U-Th)/He thermochronometry**

**Simplified assumptions** of a nominal closure temperature are not valid in regimes where **cooling rates are slow**. **The effective bulk closure temperature of a mineral decreases sharply (in situations of protracted slow cooling at rates of <1 °C/My, AHe closure temperatures as low as 30 °C have been reported (Flowers et al., submitted; Soderlund et al., 2005), and grain size effects also become increasingly important as longer residence in the PRZ leads to larger disparities in calculated dates between large and small grains. We have tried to minimize this effect by selecting grains of similar size, petrographic characteristics, and morphology, but no two grains are ever identical, and U,Th zonation, while invisible to the eye can exert a large effect on the accuracy of the alpha ejection correction. The depth interval of the PRZ expands and contracts depending on the steepness of the crustal geotherm, which, in turn, is controlled by many unquantified parameters like radiogenic heat production, fluid circulation, and topographic**

evolution. Additionally, in slowly-cooling, stable cratonic geotherms, the depth extent of the PRZ expands with a decrease in geothermal gradient such that the cumulative effect of partial He-retention during slow passage through this zone can contribute a significant percentage of the measured date. This serves to add larger uncertainty to the already theoretical notion of a bulk closure temperature for a whole mineral grain.

Add to this scenario a stochastic component of sudden advective heat transport (i.e. catastrophic uplift of the Rwenzori Massif as in Figure 6, Model C) and the inherent danger of steady-state (conductive) thermal equilibrium assumptions is plainly illustrated. Because the PRZ is so close to the landsurface in a slowly-cooled terrane (<1 km for AHe) the onset of rapid exhumation driven by sudden uplift (e.g. due to delamination of dense lower crust or brittle crustal failure) would instantaneously disrupt an equilibrium geotherm, advecting it upwards without a chance for conductive thermal relaxation, where it would be exposed at the landsurface as a paleo-PRZ. (U-Th)/He dates from this section would, in effect, represent a quenched measure of some unknown period of partial He-retention accumulated in the pre-disturbance thermal structure. In order to measure dates reflecting the age of a punctuated disturbance, the magnitude of subsequent exhumation must be at least equal to the initial depth of the PRZ. In areas of recently initiated active surface uplift like the Rwenzori, this minimum condition is often not met, leaving a misleading impression at the present-day active landsurface of ancient continuous slow cooling--a relict throwback to the ancient thermal structure it upended.

In the Rwenzori there is ample evidence for the approximate timing of major uplift to substantiate Model C. A preponderance of evidence dictates that extension did not begin in the Albertine Basin until ca. 8 Ma, and uplift of the Rwenzori followed after ca. 2.5 Ma. Even though we do not see sufficient exhumation to expose young ages anywhere in the range yet, sample R416 provides a tantalizing hint that they are close to the surface today. Whereas all the other AHe dates measured throughout the Rwenzori are Cretaceous, those from R416 date from the Miocene. Its ZHe dates show similarly distinctive young ages relative to the rest of the range. This is an expected result of its structural position at the base of the active scarp that forms the western slope of the massif; of all our sample locations it is here that we expect maximal denudation to have occurred. In this case, the ages still predate uplift despite their relative youth, suggesting that either they have experienced partial resetting due to recent shallow thermal perturbation related to extension and volcanism in the Albertine Basin while



residing in the shallow crust above the cratonic PRZ. Alternatively, they could have come from a deeper structural level, having recently penetrated through the base of the PRZ before initiation of uplift accelerated their passage through the PRZ to the surface.

The interesting corollary to the young ages of R416 is that the uniformly old ages measured for the rest of the samples suggest that they all shared similar cooling and exhumation histories regardless of their structural location within the Rwenzori block. While there are many small factors that we can expect to lead to large disparities in measured ages under conditions of protracted slow cooling (e.g. spatial or temporal variations in exhumation, heat production, chemical zonation, He-saturation), when considered broadly, the consistency of AHe and Zhe dates across the range indicate that the likeliest explanation is a regionally uniform thermal evolution--from slow cooling to rapid uplift and erosion while maintaining spatially uniform exhumation rates in order to exposure comparable structural depths across the upper slopes and entire eastern flank of the range (Figure 7). These results also lend support to the notion that the massif has the structure of a bent plate as it was described by early workers rather than a true horst with opposing active scarps as it has often been referred to more recently.

Even though the (U-Th)/He ages do not directly record the timing and rate of Rwenzori uplift/exhumation, they still place a robust upper bound on the magnitude of erosion that has occurred since the Cretaceous. This, in turn, enables us to better constrain estimates of exhumation rate based on other temporal observations. The first evidence of extension in the Albertine Basin is marked by ca. 8 Ma fluvial sedimentation within a subsiding shallow axial basin that eventually became the site of paleolake Obwerka extending over the entire region encompassing today's Lakes Albert, Edward, and George (Laerdal, 2000; Hopwood and Lepage, 1953). Based on the biostratigraphic work of Pickford et al. (1992), the Rwenzori rose from beneath this local base level to their present altitude within the last 2.5 My, requiring a minimum average uplift rate of 1.6 km/My. In all likelihood, major uplift occurred even more recently, related to initiation of volcanism and drainage reversal in the middle Pleistocene. This would require a time averaged exhumation rate of 35 km/My--a rate comparable to that of horizontal plate motions. Our thermochronological data is consistent with such recent and rapid uplift of the Rwenzori block, but it cannot constrain the timing any better than setting a maximum limit of total exhumation that has occurred since the closure of He-diffusion in apatites.

Because uplift occurred so recently and rapidly, erosion has not yet had a chance to 'catch up,' resulting in preservation of trademark high-elevation relict surfaces and the muted local relief often observed on the Rwenzori. The fact that erosion has not kept pace with uplift over the brief lifespan of the Rwenzori does not imply that the massif is not eroding at a rapid rate. Rather, it should be taken as further testament to the incredible rate and magnitude of uplift that has created the Rwenzori massif. Given its climate, high relief, huge annual rainfall, and glacial activity, the erosive potential of the Rwenzori is enormous and easily observed in the field in the form of bedrock landslides, thin (or no) soil cover, and steep, narrow, bouldery river channels. The younger the topography of the range, the higher a rate of erosion that could be accommodated while still keeping net exhumation under 2 km.

### **Possible driving mechanisms**

(U-Th)/He thermochronology provides a powerful constraint on the timing and mechanism(s) that can be invoked to explain the enigmatic Rwenzori uplift. For example, it is difficult to derive an isostatic model for uplift based on feedback from accelerated glacial erosion because the AHe ages require that the amount of surface uplift greatly exceeded the net erosion experienced over the life of the range. Other possible mechanisms that could allow for rapid development of local relief in an extensional setting include rebound from delamination of dense lower crust (e.g. Ghosh et al., 2006), cracking of attenuated lithosphere (e.g. ten Brink et al., 1997), or localized compression in the transfer zone between oblique rift segments (e.g. Ebinger 1989b). The mechanism must also allow, or better, account for initiation of late, small-volume **ultrapotassic** magmatism and provide for tightly restricted uplift expression limited to the **Rwenzori** horst. The young dates observed at the lowest elevation along the Congolese slope of **the Rwenzori** range (representing the deepest structural level exhumed in the range) suggest the **presence** of a thermal anomaly responsible for the partial resetting both the AHe and ZHe **systems**. Upper Pleistocene to Holocene volcanic vents and cones as well as thermal springs **scattered** around the periphery of the rift-flank attest to this. A likely explanation is that a **thermal pulse** resulting (or deriving) from extension in the Albertine Basin has reached shallow crustal levels, but the transient perturbation has not yet made it to the surface. In the end, reconciling the thermochronometric data with realistic tectonic models can be reduced to trade-offs between pre-rift cooling rate, assumed cratonic geotherm, and rate and duration of surface uplift and exhumation.

## **CONCLUSIONS**

Thermochronologic work coupled with field and remote sensing observations make the case for recent and rapid non-steady state uplift of the Rwenzori massif within the last 2.5 My. Because the (U-Th)/He ages determined in this study clearly predate rift-flank uplift, they place an upper bound on the magnitude of erosion that has occurred since the Cretaceous, but, unfortunately, cannot directly specify when or how fast the exhumation was actually accomplished within that interval. For an estimation of exhumation rates we must look to outside constraints on uplift timing in order to narrow the range of plausible rates. Less than 2 km of erosion has accompanied surface uplift on the order of 5 km, leading to apparently 'old' (U-Th)/He ages. These ages reflect the non-steady state upward advection of a stable pre-rift continental geotherm documented using medium- and high-temperature thermochronometry of the U-Pb system. Assessing the relative contribution of advective versus conductive heat transport is critical in determining whether traditional unroofing rates based on thermodynamic steady state can be reliably calculated. Extremely rapid surface uplift rates are corroborated by biostratigraphic and geomorphological observations, suggesting that the Rwenzori mountains are in a transient state of topographic development. Low-relief relict landsurfaces and low-gradient stream channels presently preserved at high elevation are testament to the incapacity of erosion to keep pace with uplift during the development of the Rwenzori. Nonetheless, erosion is clearly quite a significant force on the landscape. Zones of high channel steepness observed along active faults at the base of the range indicate that landscape adjustment is occurring locally and may be in a **transient state** of upslope propagation to eventually establish a new topographic **steady state**. **The results highlight the shortcomings of models that automatically simulate young orogenic systems using the simplifying assumptions of topographic steady state.**

## **REFERENCES**

Baker, B.H., Mitchell, J.G., and Williams, L.A., 1988, Stratigraphy, geochronology and volcano-tectonic evolution of the Kedong-Naivasha-Kinangop region, Gregory Rift Valley, Kenya: *Journal of the Geological Society of London*, v. 145, p. 107-116.

- Baker, B.H., Williams, L., Miller, J., and Fitch, F., 1971, Sequence and geochronology of the Kenya rift volcanics: *Tectonophysics*, v. 11, p. 191-215.
- Batt, G.E., 2001, The approach to steady-state thermochronological distribution following orogenic development in the Southern Alps of New Zealand: *American Journal of Science*, v. 301, p. 374-384.
- Batt, G.E., Brandon, M.T., Farley, K.A., and Roden-Tice, M., 2001, Tectonic synthesis of the Olympic Mountains segment of the Cascadia wedge, using two-dimensional thermal and kinematic modeling of thermochronological ages: *Journal of Geophysical Research Solid Earth*, v. 101, p. 3333-3359.
- Beadle, L.C., 1981, *The Inland Waters of Tropical Africa, An Introduction to Tropical Limnology*: London, Longman, 475 p.
- Bellieni, G.E., 1981, Oligocene transitional tholeiitic magmatism in North Turkana (Kenya): comparison with coeval Ethiopian volcanism: *Bulletin of Volcanology*, v. 44, p. 411-427.
- Boven, A., Pasteels, P., Punzalan, L.E., Yamba, T.K., and Musisi, J.H., 1998, Quaternary perpotassic magmatism in Uganda (Toro-Ankole Volcanic Province): age assessment and significance for magmatic evolution along the East African Rift: *Journal of African Earth Sciences*, v. 26, p. 463-476.
- Braun, J., 2002, Quantifying the effect of recent relief changes on Age-elevation relationships: *Earth and Planetary Science Letters*, v. 200, p. 331-343.
- Cahen, L., Snelling, I., 1984, *The Geochronology and Evolution of Africa*: Oxford, Clarendon Press, 591 p.
- Dixey, F., 1945, Erosion and tectonics in the East African Rift System: *Quarterly Journal of the Geological Society of London*, v. 102, p. 339-388.
- Dodson, M.H., 1973, Closure temperature in cooling geochronological and petrological systems: *Contributions to Mineralogy and Petrology*, v. 40, p. 259-274.
- Doornkamp, J.C., and Temple, P.H., 1966, Surface, drainage and tectonic instability in part of southern Uganda, *Geographical Journal*, 132, Part 2, p. 238-252..
- Drake, R.E., Van Couvering, J.A., Pickford, M.H., Curtis, G.H., and Harris, J.A., 1988, New chronology for the early Miocene mammalian faunas of Kisingiri, western Kenya: *Journal of the Geological Society of London*, v. 145, p. 479-491.
- Ebinger, C.J., 1989a, Geometry and kinematics of border faults and accommodation zones, Kivu-Rusizi rift, Africa: *Tectonics*, v. 8, p. 117-133.,
- , 1989b, Tectonic development of the western branch of the East African Rift System: *Geological Society of America Bulletin*, v. 101, p. 885-903.
- Egoroff, B., 1966, Contribution a l'etude du gabbro et des amphiboloschistes du ruwenzori: In *Exploration du Parc National Albert*, v 20, Institut Des Parcs Nationaux du Congo, 101 p.
- Farley, K.A., 2000, Helium diffusion from apatite: General behavior as illustrated by Durango fluorapatite: *Journal of Geophysical Research*, v. 105, p. 2903-2914.
- Filippi, F.D., 1908, *Ruwenzori: An account of the expedition of H.R.H Prince Luigi Amedeo of Savoy, Duke of Abruzzi*: E.P. Dutton, New York, 403 p.
- Flowers, R.M., Bowring, S.A., and Reiners, P.W., 2006, Low long-term erosion rates and extreme continental stability documented by ancient (U-Th)/He dates: *Geology*, submitted.
- Ghosh, P., Garzzone, C.N., and Eiler, J.M., 2006, Rapid uplift of the Altiplano revealed through  $^{13}\text{C}$ - $^{18}\text{O}$  bonds in paleosol carbonates: *Nature*, v. 311, p. 511-515.

- Hepworth, J.V., 1962, The relative ages of plateau and plain in West Nile District as indicated by Quaternary erosion surfaces, p. 37-45.
- Hopwood, A., and Lepersonne, J., 1953, Presence de formations d'age miocene inferieur dans le fosse tectonique du lac Albert: *Annals Societe Geologique Belge*, v. 77.
- Hodges, K.V., 2003, Geochronology and thermochronology in orogenic systems. In R. Rudnick (ed), *Treatise on Geochemistry*, v. 3, p. 263-292.
- House, M.A., Kelley, S.A., and Roy, M., 2003, Refining the footwall cooling history of a rift flank uplift, Rio Grande rift, New Mexico: *Tectonics*, v. 22, 18 p.
- House, M.A., Farley, K.A. and Kohn, B.P. 1999, An empirical test of helium diffusion in apatite: borehole data from the Otway Basin, Australia: *Earth and Planetary Science Letters*, v. 170, p. 463-474.
- Kampunzu, A.B., Bonhomme, M.G., and Kanika, M., 1998, Geochronology of volcanic rocks and evolution of the Cenozoic Western Branch of the East African Rift System: *Journal of African Earth Sciences*, v. 26, p. 441-461.
- Kiconco, L., 2005, The Semliki Basin, Uganda: Its sedimentation history and stratigraphy in relation to petroleum accumulation: MSc Thesis, University of Cape Town, 167 p.
- Laerdal, T., 2000, Lakes Edward, George, and Victoria (Uganda): A study of Late Quaternary rift tectonics, sedimentation and paleoclimate: PhD Thesis, University of Bergen, 163 p.
- Laerdal, T., and Talbot, M.R., 2002, Basin neotectonics of Lakes Edward and George, East African Rift: *Palaeogeography Palaeoclimatology Palaeoecology*, v. 187, p. 213-232.
- Maasha, N., 1975a, Seismicity and Tectonics of Uganda: *Tectonophysics*, v. 27, p. 381-393.
- , 1975b, Seismicity of Ruwenzori Region in Uganda: *Journal of Geophysical Research*, v. 80, p. 1485-1496.
- McConnell, R.B., 1959, Outline of the geology of the Ruwenzori Mountains: a preliminary account of the results of the British Ruwenzori expedition 1951-1952: *Overseas Geology and Mineral Resources*, v. 7, p. 245-268.
- , 1972, Geological development of the rift system of East Africa: *Geological Society of America Bulletin*, v. 83, p. 2549-2572.
- Michot, P., 1934, Le Ruwenzori et la peneplaine du centre africain: *Institut Royal Colonial Belge Memoires*, v. 54, p. 5-37.
- Morley, C.K., Wescott, W.A., Stone, D.M., Harper, R.M., Wigger, S.T., and Karanja, F.M., 1992, Tectonic Evolution of the Northern Kenyan Rift: *Journal of the Geological Society*, v. 149, p. 333-348.
- Ollier, C.D., 1990, Morphotectonics of the Lake Albert Rift Valley and its significance for continental margins: *Journal of Geodynamics*, v. 11, p. 343-355.
- Pickford, M., Senut, B., Ambrosi, J.P., Dechamps, R., Faure, M., Vandamme, D., Texier, P.J., Baguma, Z., and Musiime, E., 1992, Revision of the Neogene Biostratigraphy of the Western Rift, Uganda Zaire: *Comptes Rendus De L Academie Des Sciences Serie Ii*, v. 315, p. 1289-1292.
- Reiners, P.W., 2005, Zircon (U-Th)/He thermochronometry. In Reiners, P.W. and Ehlers, T.A. (eds) *Reviews in Mineralogy and Geochemistry*, v. 58, p. 151-179.
- Reiners, P.W., and Brandon, M.T., 2006, Using thermochronology to understand orogenic erosion: *Annual Review of Earth and Planetary Science*, v. 34, p. 419-466.
- Reiners, P.W., Spell, T.L., Nicolescu, S., and Zanetti, K.A., 2004, Zircon (U-Th)/He thermochronometry: He diffusion and comparisons with  $^{40}\text{Ar}/^{39}\text{Ar}$  dating: *Geochimica et Cosmochimica Acta*, v. 68, p. 1857-1887.

- Saggerson, E.P., and Baker, B. H., 1965, Post-Jurassic erosion surfaces in eastern Kenya and their deformation in relation to rift structure: *Quarterly Journal of the Geological Society of London*, v. 121, p. 5-72.
- Schmitz, M.D., and Bowring, S.A., 2003, Constraints on the thermal evolution of continental lithosphere from U-Pb accessory mineral thermochronometry of lower crustal xenoliths, southern Africa: *Contributions to Mineralogy and Petrology*, v. 144, p. 592-618.
- Shackleton, R.M., 1951, A contribution to the geology of the Kavairondo Rift Valley: *Quarterly Journal of the Geological Society of London*, v. 106, p. 345-392.
- Soderlund, P., Juez-Larre, J., Page, L.M., and Dunai, T.J., 2005, Extending the time range of apatite (U-Th)/He thermochronometry in slowly cooled terrains: *Earth and Planetary Sciences*, v. 239, p. 266-275.
- Stankiewicz, J., and de Wit, M.J., 2006, A proposed drainage evolution model for central Africa-Did the Congo flow east? *Journal of African Earth Science*, In Press.
- Tanner, P.W.G., 1971, The Stanley Volcanics Formation of Ruwenzori, Uganda: *Annual Report of the Research Institute of African Geology*, v. 15, p. 8-11.
- ten Brink, U.S., Hackney, R.I., Bannister, S., Stern, T.A., and Makovsky, Y., 1997, Uplift of the Transantarctic Mountains and the bedrock beneath the East Antarctic ice sheet: *Journal of Geophysical Research*, v. 102, p. 27603-27621.
- Van Damme, D., and Pickford, M., 2003, The late Cenozoic Thiaridae (Mollusca, Gastropoda, Cerithioidea) of the Albertine Rift Valley (Uganda-Congo) and their bearing on the origin and evolution of the Tanganyikan thalassoid malacofauna: *Hydrobiologia*, v. 498, p. 1-83.
- van der Beek, P.A., Cloetingh, S., and Andriessen, P.A.M., 1994, Extensional basin formation mechanisms and vertical motion of rift flanks: constraints from tectonic modeling and fission-track thermochronology: *Earth and Planetary Science Letters*, v. 121, p. 417-433.
- Watts, A.B., Karner, G.D., and Steckler, M.S., 1982, Lithospheric flexure and the evolution of sedimentary basins. In Kent, P., Bott, M.H.P., McKenzie, D.P., and Williams, C.A. (eds), *The Evolution of Sedimentary Basins: Philosophical Transactions of the Royal Society of London*, v. 3305, p. 249-281.
- Wayland, E.J., 1934, *Penplains and some other erosional platforms: Geological Survey of Uganda, Annual Report 1933*, p. 77-79.
- Whittow, J.B., The landforms of the central Ruwenzori, east Africa, *Geographical Journal*, 132, Part 1, p. 32-42, 1966.
- Willet, S.D., Slingerland, R., and Hovius, N., 2001, Uplift, shortening and steady state topography in active mountain belts: *American Journal of Science*, v. 301, p. 455-485.
- Wolf, R.A., Farley, K.A., and Kass, D.M., 1998, Modeling the temperature sensitivity of the apatite (U-Th)/He thermochronometer: *Chemical Geology*, v. 148, p. 105-114.





Figure 1. Geographical location of the Albertine Rift Basin within the Western Branch of the East African Rift System.



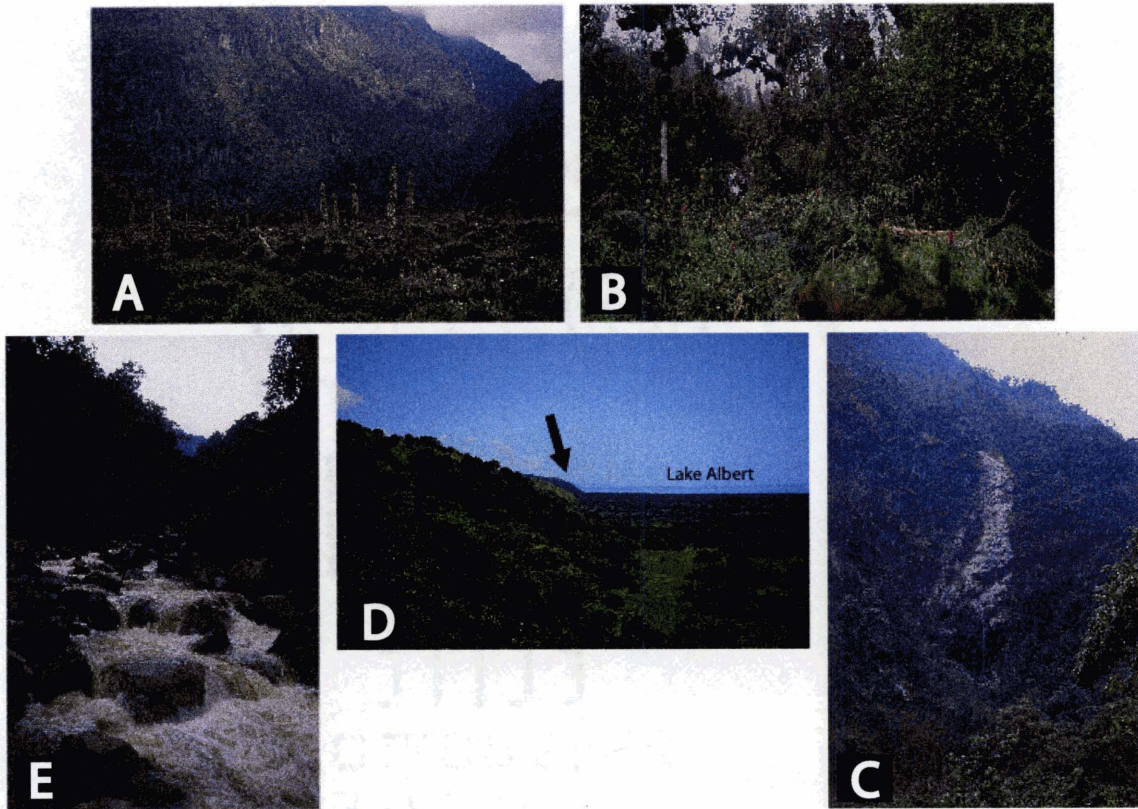
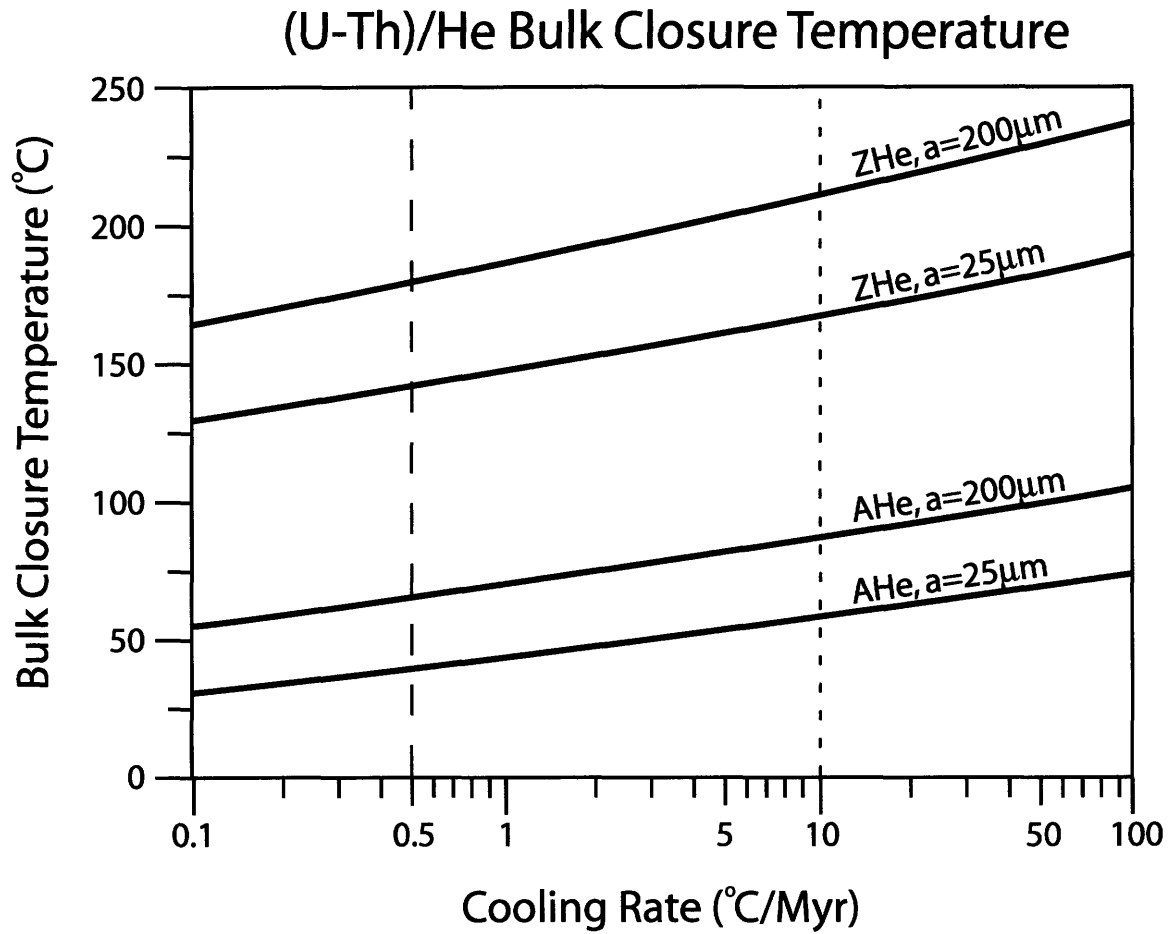


Figure 2. Some typical landscapes of the Rwenzori and surroundings

- A. Upper Bigo Bog- high-elevation flat valley with unique afroalpine flora and typically steep bedrock walls.
- B. Giant heath biota inhabits low-relief surfaces.
- C. Active mass-wasting by bedrock landslide.
- D. Rift valley scarp and plain looking south from U03-02
- E. High gradient boulder bed stream





**Figure 3.** Plot shows relationship between regional cooling rate and whole-grain bulk closure temperature for the (U-Th)/He system (after Reiners, 2005) using the equations of **Dodson (1973)** and physical constants of Farley (2000) and Reiners et al. (2004). Long dashed line marks cooling rate determined as upper limit for the Rwenzori block, dotted line depicts a commonly selected value for active orogenic terranes.

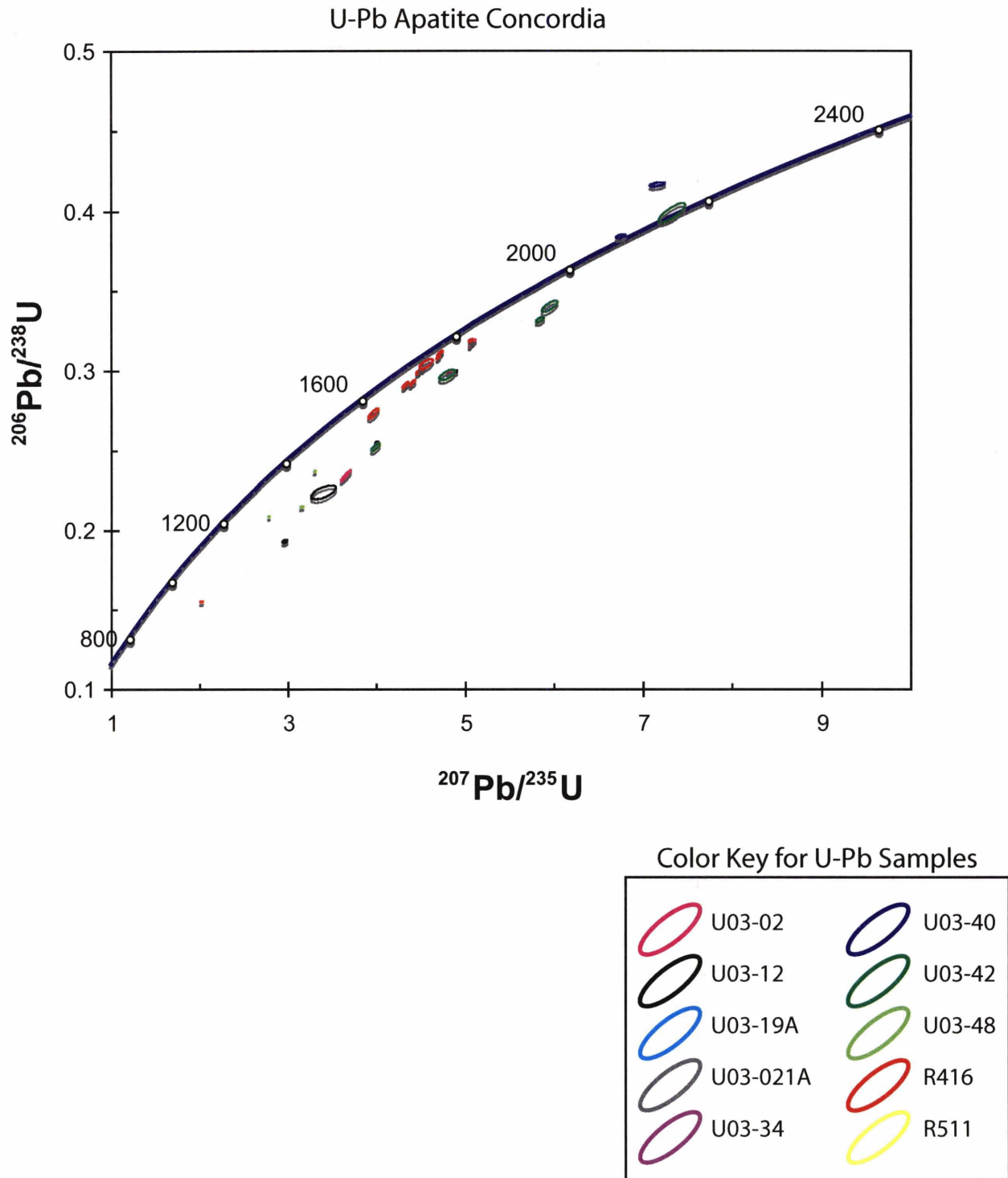


Figure 4a. U-Pb concordia diagram for apatite thermochronometry. Sample locations can be found in Figure 7.

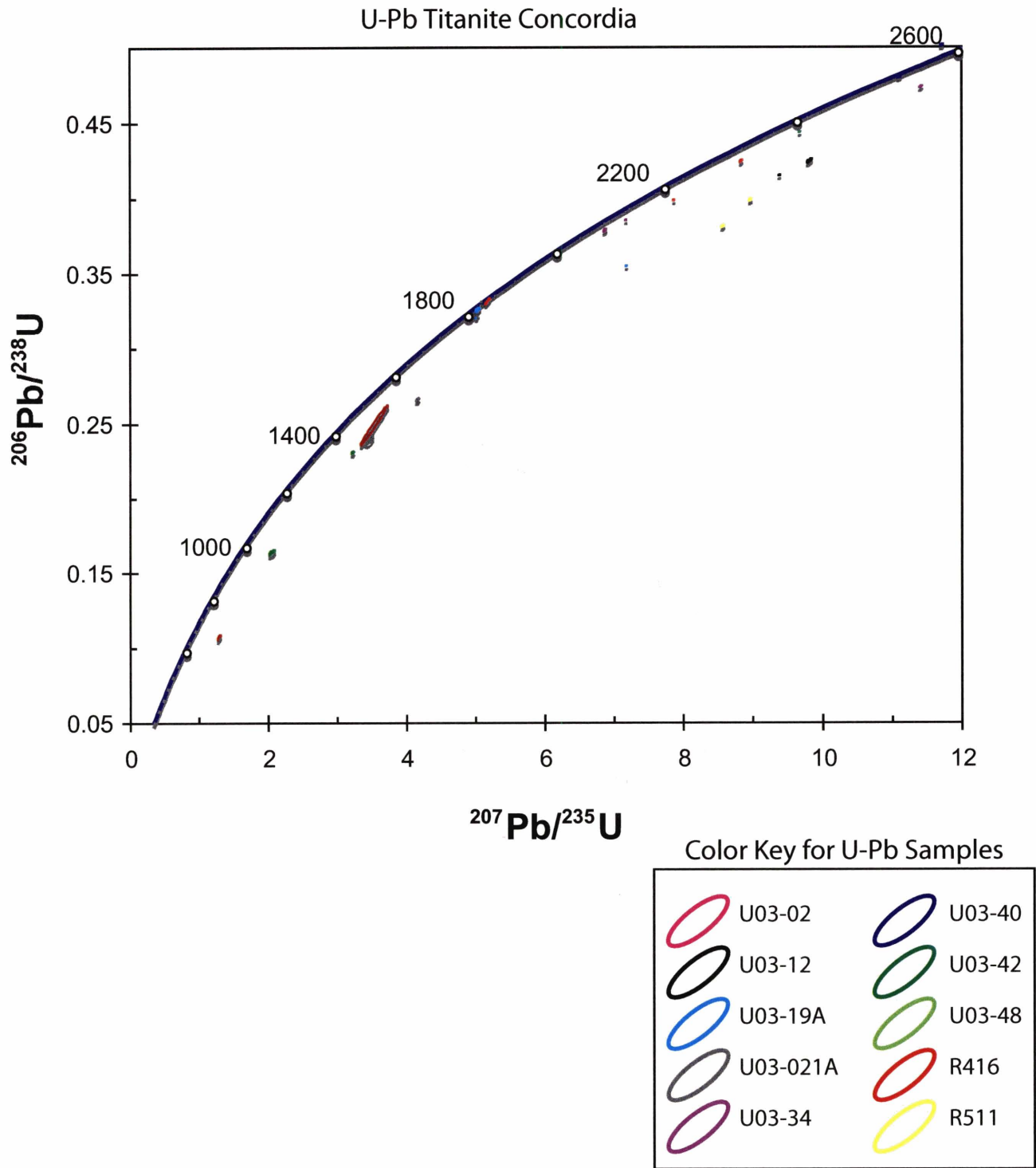


Figure 4b. U-Pb concordia diagram for titanite thermochronometry. Sample locations can be found in Figure 7.

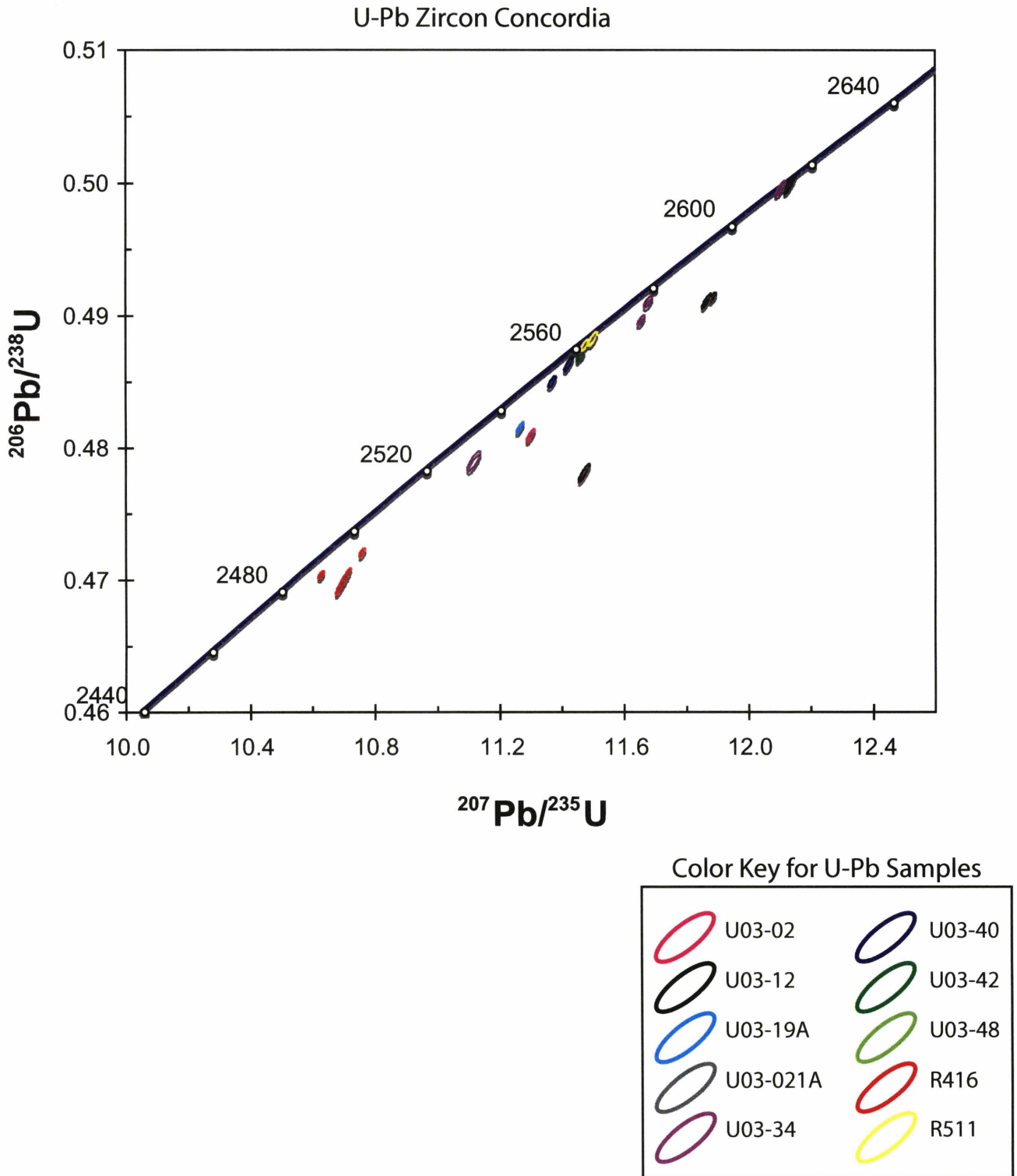


Figure 4c. U-Pb concordia diagram for zircon thermochronometry. Sample locations can be found in Figure 7.

# Thermal Evolution of the Rwenzori Basement from Combined U-Pb and (U-Th)/He Chronometry

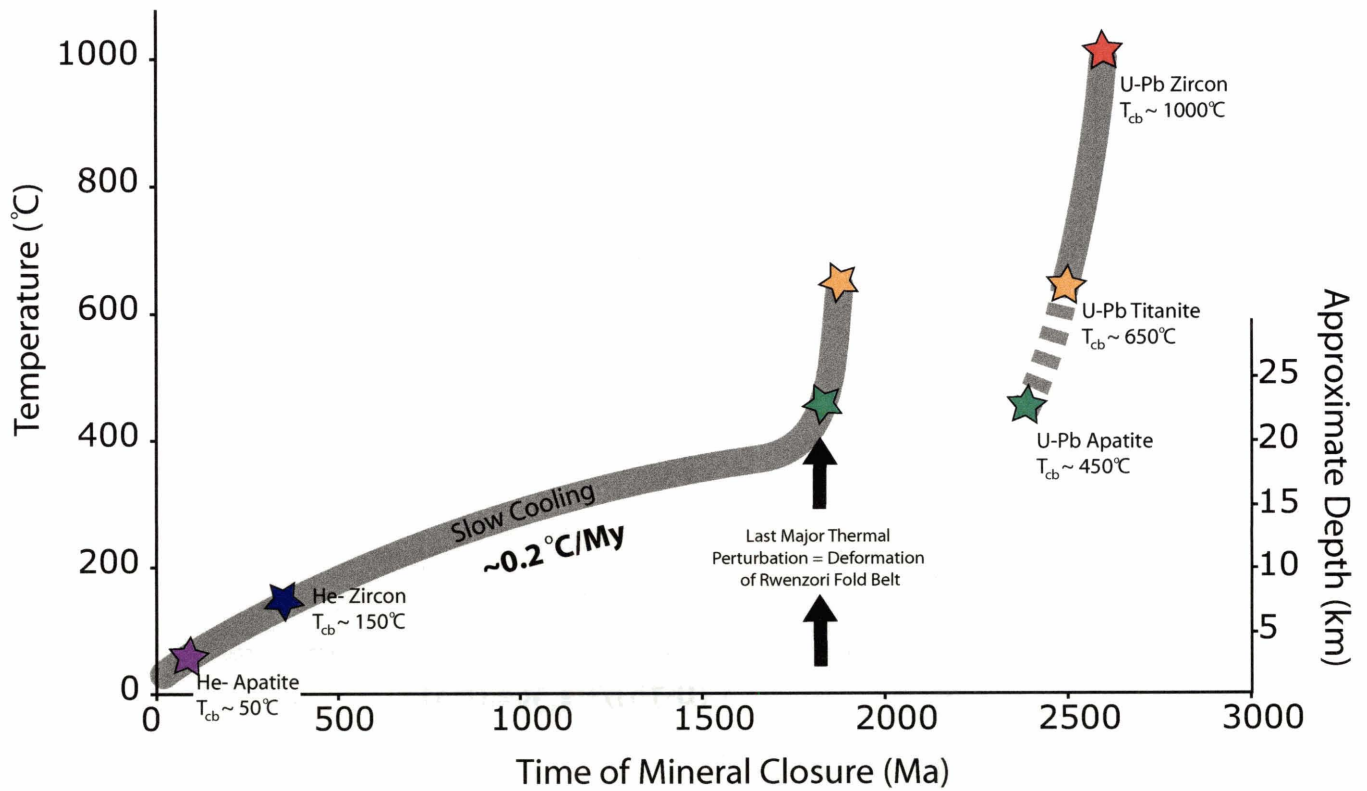


Figure 5. Generalized cooling curve generated from thermochronometric data in Tables 1 and 2.

### (U-Th)/He Age v. Elevation

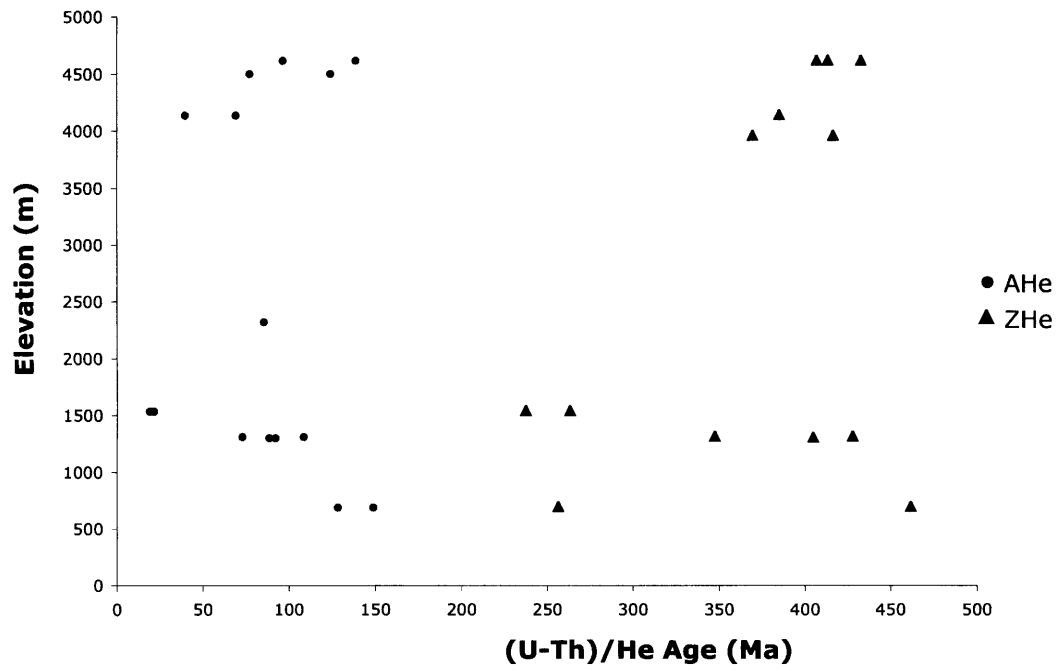


Figure 6. Plot of (U-Th)/He age of sample versus its elevation in the landscape shows lack of coherent trend.

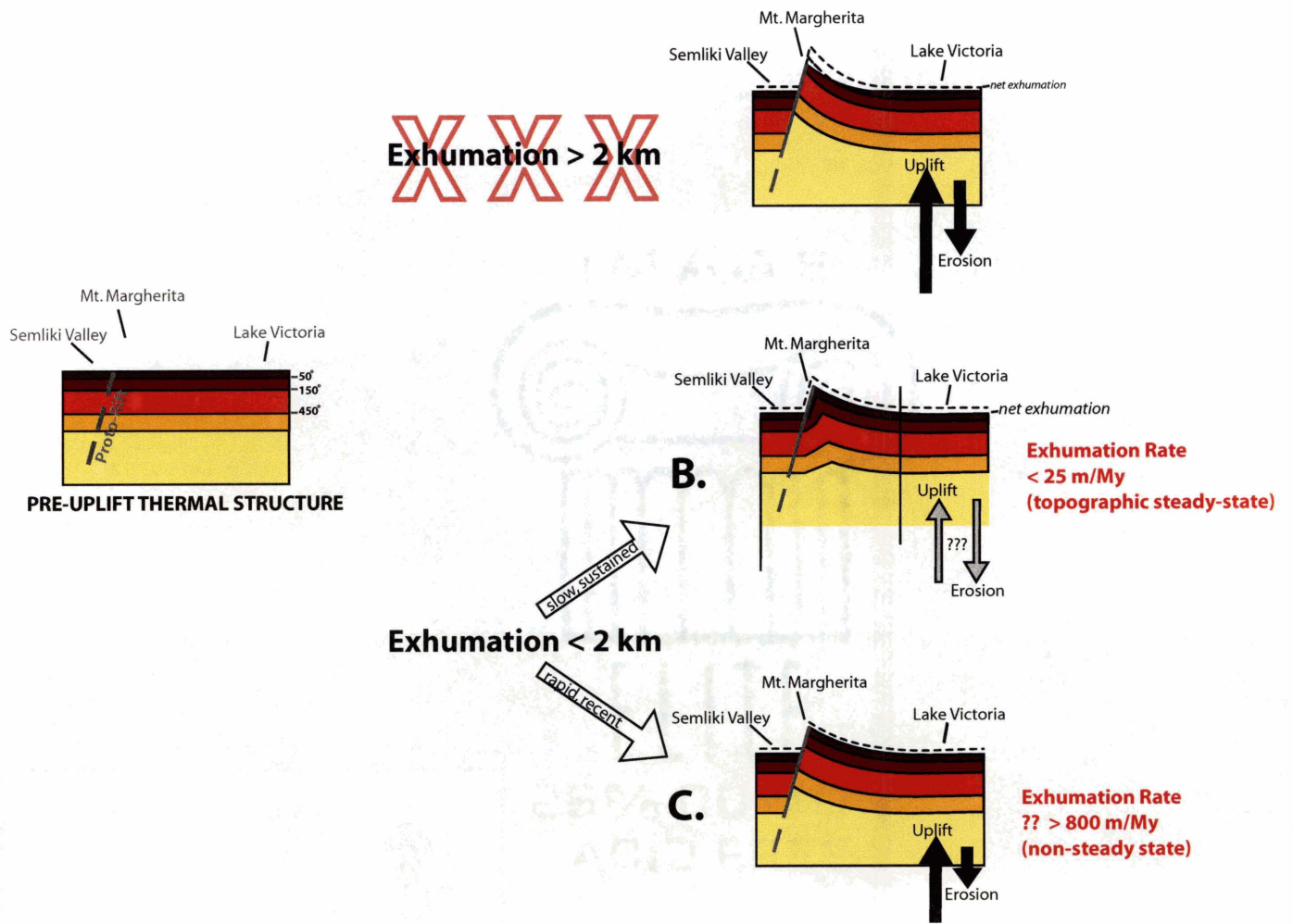


Figure 7. Models for Rwenzori Uplift and Exhumation



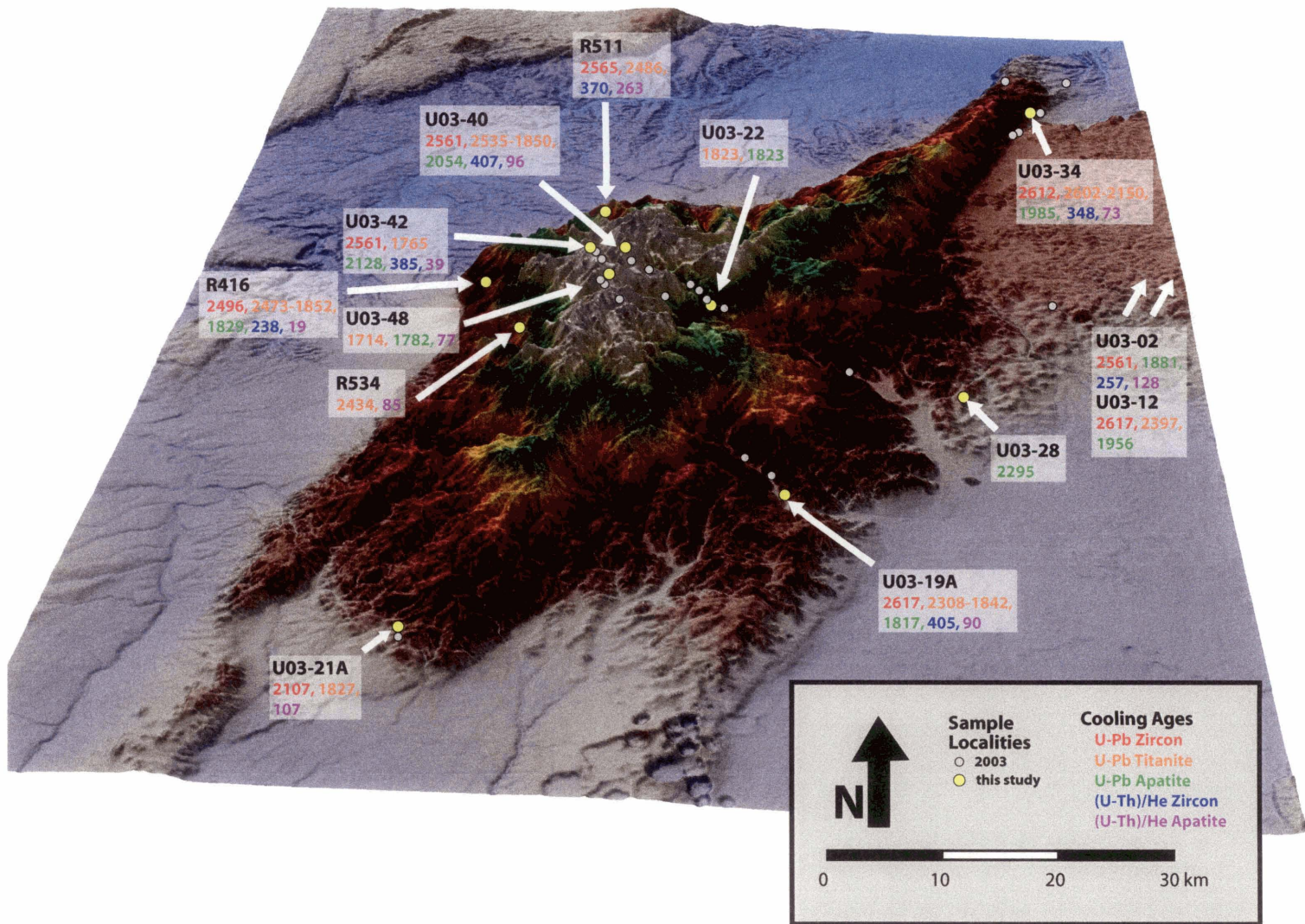


Figure 8. 3D rendering of SRTM DEM showing Rwenzori sample localities with U-Pb and (U-Th)/He cooling ages color-coded by mineral isotope system. Data can be found in Tables 1 and 2.



Table 1. U-Pb Isotopic Data

Fraction	Pb*	Pb	Th	Isotopic Ratios				Dates (Ma)				% disc.				
				206Pb*	208Pb	206Pb	238U	206Pb	238U	207Pb	235U		207Pb	206Pb		
															204Pb	206Pb
(ppg)	U			% err	% err	% err	% err	corr.	coef.	% err	% err					
<b>U03-02</b>																
<i>zircon</i>																
z1	233.4	0.4	0.60	13034	0.169	0.480958	0.08	11.29908	0.09	0.1703863	0.05	0.872	2531.4	2548.1	2561.4	1.42
z2	90.9	1.9	0.44	5228	0.138	0.424911	0.09	9.79625	0.10	0.1672094	0.06	0.833	2282.7	2415.8	2529.9	11.59
z3	58.4	5.8	0.17	3640	0.067	0.299254	0.08	5.74422	0.09	0.1392164	0.04	0.879	1687.6	1938.0	2217.5	27.11
<i>titanite</i>																
s4	0.2	26.9	5.63	19	2.178	0.456642	1.89	16.57893	2.62	0.2633171	1.79	0.732	2424.7	2910.8	3266.7	30.80
s5	0.3	55.9	2.14	22	1.486	0.209012	0.67	5.38371	1.86	0.1868137	1.64	0.492	1223.6	1882.3	2714.3	60.08
<i>apatite</i>																
a1	1.5	20.5	0.09	103	0.031	0.299477	0.34	4.82231	0.40	0.1167859	0.20	0.874	1688.7	1788.8	1907.6	13.03
a2	2.1	9.9	0.09	140	0.027	0.317398	0.58	5.07368	0.62	0.1159358	0.20	0.948	1777.0	1831.7	1894.5	7.09
a4	1.2	11.7	0.13	87	0.054	0.234424	1.23	3.64987	1.30	0.1129206	0.38	0.957	1357.6	1560.5	1846.9	29.34
<b>U03-12</b>																
<i>zircon</i>																
z1	876.0	2.0	0.73	47442	0.205	0.491122	0.09	11.86469	0.10	0.1752128	0.04	0.914	2575.5	2593.8	2608.1	1.51
z2	416.2	1.1	0.82	22098	0.233	0.491408	0.06	11.88493	0.07	0.1754095	0.04	0.805	2576.8	2595.4	2609.9	1.54
z3	103.7	3.4	0.85	4986	0.245	0.478097	0.11	11.47115	0.13	0.174016	0.05	0.910	2519.0	2562.2	2596.7	3.61
z4	366.2	1.4	0.89	19221	0.248	0.499906	0.12	12.13291	0.12	0.1760253	0.04	0.934	2613.4	2614.7	2615.8	0.11
<i>titanite</i>																
s1	3.8	37.3	3.68	125	1.165	0.424854	0.26	9.81416	0.29	0.1675377	0.12	0.907	2282.5	2417.5	2533.2	11.74
s2	5.4	107.5	1.34	240	0.428	0.415302	0.06	9.38580	0.09	0.1639101	0.07	0.700	2239.1	2376.4	2496.4	12.19
<i>apatite</i>																
a1	2.8	29.7	1.32	134	0.445	0.299654	0.18	4.89061	0.26	0.11837	0.17	0.752	1689.6	1800.6	1931.8	14.24
a2	0.3	27.0	1.89	25	0.793	0.223938	1.59	3.40008	3.34	0.1101187	2.65	0.627	1302.6	1504.4	1801.4	30.54
a3	2.6	26.8	2.95	94	1.123	0.254892	0.27	3.99951	0.36	0.1138017	0.21	0.806	1463.7	1634.1	1861.0	23.84
a5	1.3	46.7	3.19	49	1.566	0.193296	0.37	2.96124	0.71	0.1111095	0.56	0.626	1139.2	1397.7	1817.6	40.66
<b>U03-19A</b>																
<i>zircon</i>																
z1	147.8	0.5	0.70	8140	0.205	0.435044	0.17	9.28855	0.18	0.154851	0.05	0.960	2328.4	2366.9	2400.2	3.56
z2	604.3	0.4	0.21	37258	0.063	0.421490	0.09	8.74302	0.10	0.1504434	0.05	0.875	2267.2	2311.6	2351.0	4.22
z3	2501.1	0.5	0.53	141832	0.148	0.481547	0.07	11.26482	0.08	0.1696619	0.04	0.873	2534.0	2545.3	2554.3	0.96

Table 1. U-Pb Isotopic Data (cont'd)

Fraction	Pb*	Pb (pg)	Th U	Isotopic Ratios				Dates (Ma)								
				$^{206}\text{Pb}^*/^{204}\text{Pb}$	$^{208}\text{Pb}/^{206}\text{Pb}$	$^{206}\text{Pb}/^{235}\text{U}$	$^{206}\text{Pb}/^{238}\text{U}$	$^{207}\text{Pb}/^{235}\text{U}$	$^{207}\text{Pb}/^{235}\text{U}$	$^{207}\text{Pb}/^{206}\text{Pb}$	$^{206}\text{Pb}/^{206}\text{Pb}$	$\% \text{ disc.}$				
				$206\text{Pb}^*$	$208\text{Pb}$	$207\text{Pb}$	$206\text{Pb}$	$207\text{Pb}$	$206\text{Pb}$	$207\text{Pb}$	$206\text{Pb}$	$\% \text{ err}$	$\% \text{ err}$	$\% \text{ err}$	$\% \text{ err}$	
<b>U03-19A</b>																
<i>titanite</i>																
s1	3.8	17.0	2.52	155	0.738	0.326000	0.38	5.03443	0.51	0.1120036	0.33	0.773	1819.0	1825.1	1832.2	0.83
s2	5.1	99.1	3.40	176	1.018	0.322771	0.09	5.04123	0.14	0.1132768	0.11	0.666	1803.2	1826.3	1852.6	3.06
s3	12.9	51.5	0.30	710	0.104	0.355134	0.09	7.18405	0.11	0.1467153	0.05	0.871	1959.1	2134.5	2308.0	17.51
s4	4.9	14.8	2.02	209	0.599	0.320273	0.24	4.90815	0.29	0.1111465	0.16	0.831	1791.1	1803.7	1818.3	1.71
s5	6.1	23.6	2.62	222	0.790	0.320895	0.14	5.01257	0.18	0.1132912	0.10	0.815	1794.1	1821.4	1852.9	3.63
<i>apatite</i>																
a2	0.1	698.5		20	0.873					0.1168584	0.00				1908.7	100.00
<b>U03-21A</b>																
<i>zircon</i>																
z6a	8.1	0.7	0.37	509	0.107	0.386121	0.43	6.97125	0.48	0.1309442	0.19	0.916	2104.8	2107.8	2110.7	0.32
z7a	49.8	3.8	0.98	2651	0.283	0.384520	0.34	6.99268	0.42	0.1318937	0.24	0.819	2097.4	2110.5	2123.3	1.43
<i>titanite</i>																
s1	2.4	38.9	0.97	137	0.229	0.411391	0.15	6.41000	0.27	0.1130062	0.21	0.605	2221.3	2033.6	1848.3	-23.89
s2	3.0	31.2		173	0.163					0.1108712	0.00				1813.7	100.00
s3	2.2	19.7	0.57	129	0.206	0.266231	0.27	4.16017	0.37	0.1133316	0.23	0.781	1521.6	1666.2	1853.5	20.08
<i>rutile</i>																
r1	2.9	15.0	0.50	174	0.150	0.321242	0.27	4.95932	0.29	0.1119667	0.10	0.938	1795.8	1812.4	1831.6	2.24
r2	5.9	54.9	0.30	350	0.086	0.331238	0.07	5.08788	0.12	0.1114027	0.10	0.616	1844.4	1834.1	1822.4	-1.39
r3	1.6	20.7	0.29	103	0.109	0.239456	0.94	3.46045	1.33	0.1048106	0.88	0.751	1383.9	1518.3	1711.0	21.23
<b>U03-34</b>																
<i>zircon</i>																
z2	239.5	0.6	0.35	14099	0.098	0.491051	0.07	11.67704	0.09	0.1724666	0.06	0.753	2575.2	2578.9	2581.7	0.31
z3	148.4	0.4	0.64	8210	0.178	0.499610	0.10	12.10219	0.11	0.1756837	0.05	0.903	2612.1	2612.4	2612.5	0.02
z5a	162.2	1.1	0.16	9975	0.046	0.489665	0.06	11.65482	0.08	0.1726257	0.05	0.810	2569.2	2577.1	2583.3	0.66
z6a	43.9	0.6	0.12	2747	0.035	0.478998	0.13	11.11658	0.15	0.1683202	0.08	0.838	2522.9	2532.9	2541.0	0.86
<i>titanite</i>																
s1	22.8	30.5	0.99	1037	0.293	0.385625	0.06	7.17697	0.08	0.1349815	0.05	0.777	2102.5	2133.6	2163.8	3.32
s2	6.2	156.6	0.41	319	0.119	0.473911	0.13	11.41390	0.15	0.1746772	0.07	0.892	2500.7	2557.6	2603.0	4.74
s3	9.6	10.2	2.13	367	0.626	0.379024	0.20	6.87827	0.26	0.1316169	0.16	0.787	2071.7	2095.9	2119.6	2.64

Table 1. U-Pb Isotopic Data (cont'd)

Fraction	Pb* Pb <sub>c</sub>	Pb (pg)	Th U	Isotopic Ratios				Dates (Ma)				% disc.				
				<sup>206</sup> Pb/ <sup>204</sup> Pb	<sup>208</sup> Pb/ <sup>206</sup> Pb	<sup>206</sup> Pb/ <sup>238</sup> U	% err	<sup>206</sup> Pb/ <sup>238</sup> U	<sup>207</sup> Pb/ <sup>235</sup> U	<sup>207</sup> Pb/ <sup>206</sup> Pb	<sup>207</sup> Pb/ <sup>206</sup> Pb					
				cont. coef.	% err	<sup>207</sup> Pb/ <sup>206</sup> Pb	% err	cont. coef.	% err							
<b>U03-40</b>																
<i>zircon</i>																
z1	319.4	0.5	0.87	16904	0.243	0.486362	0.09	11.42162	0.10	0.1703204	0.05	0.894	2554.9	2558.2	2560.8	0.28
z2	368.8	0.4	0.74	20022	0.207	0.485024	0.07	11.36873	0.09	0.1699994	0.05	0.834	2549.1	2553.9	2557.6	0.40
<i>titanite</i>																
s1	3.0	95.3	0.12	193	0.035	0.330655	0.09	5.15810	0.18	0.1131391	0.14	0.585	1841.6	1845.7	1850.4	0.55
s2	5.7	59.4	4.54	163	1.271	0.480520	0.13	11.10210	0.18	0.1675685	0.11	0.769	2529.5	2531.7	2533.5	0.19
s3	3.3	291.8	3.25	118	0.878	0.501222	0.10	11.71479	0.16	0.1695128	0.12	0.705	2619.0	2581.9	2552.8	-3.16
s3	3.3	291.8	3.25	118	0.878	0.501222	0.10	11.71479	0.16	0.1695128	0.12	0.705	2619.0	2581.9	2552.8	-3.16
<i>apatite</i>																
a1A	0.6	109.1	2.34	38	0.658	0.384380	0.24	6.74899	0.63	0.1273434	0.53	0.584	2096.7	2079.1	2061.6	-1.99
a3A	0.4	288.2	2.50	31	0.637	0.416709	0.25	7.15937	0.96	0.1246064	0.84	0.596	2245.5	2131.5	2023.2	-13.03
<b>U03-42</b>																
<i>zircon</i>																
z1a	304.6	1.0	0.81	16318	0.226	0.486938	0.06	11.45873	0.08	0.1706717	0.05	0.808	2557.4	2561.2	2564.2	0.32
z2a	203.7	2.0	0.70	11149	0.197	0.487019	0.05	11.46292	0.07	0.1707058	0.04	0.775	2557.8	2561.6	2564.6	0.32
z3a	359.8	1.8	0.65	19885	0.183	0.487152	0.05	11.46038	0.07	0.1706214	0.04	0.782	2558.3	2561.4	2563.7	0.25
<i>titanite</i>																
s1	1.0	17.9	0.90	61	0.408	0.163753	0.72	2.04443	1.09	0.090549	0.75	0.723	977.6	1130.4	1437.2	34.43
s2	2.7	15.3	0.24	172	0.090	0.231019	0.28	3.22546	0.42	0.1012612	0.30	0.707	1339.8	1463.3	1647.4	20.66
s3	1.5	9.2	0.32	102	0.148	0.164385	0.77	2.07433	1.03	0.0915196	0.63	0.793	981.1	1140.4	1457.4	35.20
<i>apatite</i>																
a2	2.1	17.1	6.28	54	2.434	0.252306	0.76	3.98662	1.01	0.1145975	0.58	0.817	1450.4	1631.5	1873.6	25.19
a3	0.3	5.7	7.06	24	1.430	0.540278	7.59	9.61083	8.73	0.1290156	3.66	0.909	2784.6	2398.2	2084.6	-41.52
a4	0.4	19.3	2.03	32	0.571	0.399029	1.24	7.32205	1.66	0.1330842	0.99	0.805	2164.6	2151.5	2139.1	-1.40
a4new	0.7	41.0	1.16	45	0.378	0.332096	0.39	5.83606	0.62	0.1274546	0.44	0.711	1848.5	1951.8	2063.2	11.96
a5	0.7	19.3	1.05	48	0.331	0.340518	0.83	5.94703	1.19	0.1266655	0.76	0.767	1889.2	1968.1	2052.2	9.16
a6new	1.0	13.5	0.86	64	0.289	0.297508	0.89	4.79319	1.50	0.1168489	1.11	0.683	1678.9	1783.7	1908.6	13.66

Table 1. U-Pb Isotopic Data (cont'd)

Fraction	Pb*	Pb (pg)	Th	U	Isotopic Ratios						Dates (Ma)						
					$\frac{^{206}\text{Pb}}{^{204}\text{Pb}}$		$\frac{^{207}\text{Pb}}{^{235}\text{U}}$		$\frac{^{206}\text{Pb}}{^{238}\text{U}}$		$\frac{^{207}\text{Pb}}{^{235}\text{U}}$		$\frac{^{206}\text{Pb}}{^{238}\text{U}}$		$\frac{^{207}\text{Pb}}{^{206}\text{Pb}}$		% disc.
					corr.	% err	corr.	% err	corr.	% err	corr.	% err	corr.	% err	corr.	% err	
<b>U03-48</b>																	
<i>titanite</i>																	
s1	1.8	1.9	1.07	107	0.375	0.249230	4.37	3.53355	4.53	0.1028279	0.73	0.987	1434.5	1534.8	1675.8	16.05	
s2	3.5	3.2	0.41	195	0.271	0.107375	1.20	1.28967	1.36	0.0871109	0.54	0.917	657.5	841.1	1362.9	54.39	
<i>apatite</i>																	
a1	0.8	135.3	0.82	52	0.346	0.214876	0.13	3.14984	0.45	0.1063164	0.40	0.529	1254.7	1445.0	1737.2	30.53	
a2	2.3	64.3	0.50	137	0.193	0.208837	0.10	2.77828	0.20	0.0964866	0.16	0.593	1222.6	1349.7	1557.2	23.57	
a3	2.1	70.9	0.53	129	0.190	0.237134	0.16	3.29620	0.23	0.1008132	0.16	0.734	1371.8	1480.2	1639.1	18.09	
<b>R416</b>																	
<i>zircon</i>																	
z1a	20.4	16.5	0.21	1267	0.059	0.469915	0.17	10.69805	0.18	0.1651143	0.05	0.955	2483.2	2497.3	2508.7	1.23	
z2a	239.7	1.3	0.09	15084	0.025	0.472088	0.05	10.75815	0.07	0.1652774	0.04	0.786	2492.7	2502.5	2510.4	0.85	
z3a	353.2	1.0	0.15	21942	0.041	0.470400	0.05	10.62729	0.07	0.1638526	0.04	0.751	2485.3	2491.1	2495.8	0.51	
<i>titanite</i>																	
s1	5.5	3.9	0.09	355	0.027	0.331749	0.52	5.17944	0.54	0.1132328	0.13	0.969	1846.9	1849.2	1851.9	0.31	
s2	32.3	3.3	0.75	1643	0.220	0.424885	0.15	8.83615	0.16	0.150831	0.06	0.933	2282.6	2321.2	2355.4	3.67	
s3	41.2	9.6	1.16	1849	0.347	0.398821	0.06	7.86852	0.08	0.1430913	0.05	0.817	2163.6	2216.1	2265.0	5.27	
<i>apatite</i>																	
a3	2.3	9.0	0.36	145	0.113	0.291178	0.54	4.32460	0.63	0.1077174	0.31	0.873	1647.4	1698.1	1761.2	7.32	
a4	2.0	26.2	0.34	128	0.104	0.308476	0.24	4.69319	0.31	0.110343	0.17	0.829	1733.2	1766.0	1805.1	4.54	
a5a	2.1	14.9	0.45	132	0.138	0.301674	0.36	4.52576	0.45	0.1088059	0.24	0.841	1699.6	1735.7	1779.5	5.11	
a5b	2.2	16.8	0.47	134	0.144	0.299026	0.31	4.46354	0.40	0.1082605	0.23	0.814	1686.5	1724.2	1770.4	5.38	
a6	2.5	8.6	0.35	155	0.112	0.292444	0.53	4.40214	0.61	0.1091743	0.28	0.888	1653.7	1712.7	1785.7	8.37	
a7	1.9	12.0	0.39	119	0.118	0.310892	0.48	4.71236	0.56	0.1099329	0.26	0.886	1745.1	1769.4	1798.3	3.38	
a8	1.4	40.8	0.26	88	0.081	0.319092	0.22	5.06278	0.42	0.1150725	0.33	0.636	1785.3	1829.9	1881.0	5.82	
a9	1.3	8.6	0.45	90	0.146	0.273307	0.94	3.96135	1.19	0.1051214	0.66	0.830	1557.6	1626.3	1716.4	10.41	
a10	0.6	92.9	0.23	49	0.116	0.155223	0.17	2.01407	0.63	0.0941056	0.56	0.510	930.2	1120.3	1510.3	41.20	
a11	1.0	12.2	0.40	74	0.122	0.304417	0.82	4.55657	1.34	0.1085594	0.97	0.698	1713.2	1741.4	1775.4	3.99	

Table 1. U-Pb Isotopic Data (cont'd)

Pb*	Pb	Th	Isotopic Ratios				Dates (Ma)										
			$\frac{206\text{Pb}}{204\text{Pb}}$	$\frac{208\text{Pb}}{206\text{Pb}}$	$\frac{206\text{Pb}}{235\text{U}}$	$\frac{207\text{Pb}}{235\text{U}}$	$\frac{206\text{Pb}}{235\text{U}}$	$\frac{207\text{Pb}}{235\text{U}}$	$\frac{207\text{Pb}}{206\text{Pb}}$	$\frac{207\text{Pb}}{206\text{Pb}}$	% disc.						
Fraction Pb <sub>c</sub>	(pg)	U			% err		% err	corr.	% err	coeff.							
<b>R511</b>																	
<i>zircon</i>																	
	z1a	81.3	1.0	0.74	4435	0.206	0.487797	0.07	11.47403	0.09	0.1705985	0.05	0.800	2561.1	2562.5	2563.5	0.11
	z2a	83.1	2.2	0.72	4547	0.200	0.486274	0.09	11.49915	0.10	0.1708053	0.06	0.821	2563.2	2564.5	2565.6	0.11
<i>titanite</i>																	
	s1	39.6	3.1	0.72	1955	0.239	0.399058	0.15	8.96613	0.17	0.162955	0.08	0.870	2164.7	2334.6	2486.6	15.22
	s3	97.9	7.8	0.52	4814	0.180	0.381596	0.17	8.57511	0.18	0.1629802	0.05	0.965	2083.7	2293.9	2486.8	18.94

Table 2. (U-Th)/He data for zircon and apatite

Sample	Mass (ug)	U ppm	Th ppm	Sm ppm	Th/U	4He (nmol/g)	Raw Age (Ma)	Est 2σ +/- (Ma)	HAC	Corr. Ag (Ma)	Est 2σ +/- (Ma)
<i>Apatite Analyses</i>											
U03-02	Butiaba granite (690 m)										
a1	0.96	39	1	81	0.015	19.41	91.03	2.41	0.61	148.61	3.94
a2	1.13	74	27	201	0.375	36.30	82.90	2.04	0.65	128.21	3.16
U03-19A	Kilembe paragneiss (1300 m)										
aA	2.39	12	19		1.65		61.95	1.11	0.70	88.49	5.31
aB	1.45	11	18		1.58		58.02	1.15	0.63	92.10	5.53
U03-34	Bwamba grey granite (1310 m)										
aA	1.29	4	1		0.18		67.13	3.24	0.62	108.46	6.51
aB	3.26	10	1		0.10		53.57	1.18	0.74	72.88	4.37
U03-40	Mt. Speke gneiss (4620 m)										
a1	0.91	3	3	15	1.11	1.19	58.76	5.89	0.61	96.41	9.66
a2	1.61	6	13	30	2.35	4.33	91.20	6.87	0.66	138.58	10.44
U03-42	Stuhlmann Pass quartzite (4140 m)										
a9	13.60	5	4	42	0.826	1.07	33.16	0.75	0.84	39.36	0.89
a8	7.57	3	1	98	0.422	0.96	53.67	1.41	0.78	69.03	1.82
U03-48	Mt. Baker amphibolite (4505 m)										
aA	2.27	17	8		0.49		85.25	1.65	0.69	123.91	7.43
aB	1.70	13	5		0.38		51.10	1.11	0.66	77.19	4.63
R416	Lower Luzilubu Valley gneiss (1535 m)										
a1	2.30	18	5	34	0.31	1.37	13.36	0.36	0.71	18.87	0.50
a2	1.45	24	5	82	0.21	1.90	14.03	0.37	0.66	21.38	0.57
R511	Roccati Pass gneiss (3960 m)										
a1	2.19	15	32	27	2.22	21.41	176.14	4.29	0.67	262.52	6.39
<i>Zircon Analyses</i>											
U03-02	Butiaba granite (690 m)										
z4	2.66	755	93		0.126	794.24	186.59	4.50	0.73	256.71	6.19
z5	2.01	720	446		0.635	1466.00	320.49	7.41	0.69	462.09	10.68
U03-19A	Kilembe paragneiss (1300 m)										
zA	3.18	394	190		0.48		288.09	8.47	0.71	405.19	32.42
U03-34	Bwamba grey granite (1310 m)										
z8	2.01	162	24		0.151	222.83	240.69	5.80	0.69	348.06	8.38
z9	17.14	203	58		0.291	434.38	359.92	8.64	0.84	428.36	10.28
U03-40	Mt. Speke gneiss (4620 m)										
zA	7.45	243	180		0.74		314.35	8.61	0.77	407.19	32.58
z5	5.87	368	234		0.653	802.59	341.72	7.92	0.79	432.96	10.03
z6	6.17	312	171		0.561	630.84	322.79	7.73	0.78	413.73	9.90
U03-42	Stuhlmann Pass quartzite (4140 m)										
z6	10.23	347	221		0.654	691.30	312.69	7.24	0.81	385.34	8.93
R416	Lower Luzilubu Valley gneiss (1535 m)										
z4	2.49	419	35		0.085	441.59	188.79	4.56	0.72	263.71	6.37
z6	4.89	626	74		0.121	633.92	179.99	4.33	0.76	237.97	5.72
R511	Roccati Pass gneiss (3960 m)										
z4	4.50	354	208		0.601	688.94	308.57	7.20	0.74	416.77	9.73
z5	12.17	257	160		0.639	494.02	302.81	6.97	0.82	369.86	8.51